EDI electron time-of-flight measurements on Equator-S

G. Paschmann, N. Sckopke, H. Vaith, J. M. Quinn, O. H. Bauer, W. Baumjohann, W. Fillius, G. Haerendel, S. S. Kerr, C. A. Kletzing, et al.

Ann. Geophysicae 17, 1513–1520 (1999) © EGS – Springer-Verlag 1999

Annales Geophysicae

EDI electron time-of-flight measurements on Equator-S

G. Paschmann[1], N. Sckopke[1], H. Vaith[1], J. M. Quinn[2], O. H. Bauer[1], W. Baumjohann[1], W. Fillius[3], G. Haerendel[1], S. S. Kerr[3], C. A. Kletzing[4], K. Lynch[2], C. E. McIlwain[3], R. B. Torbert[2], E. C. Whipple[5]

[1] Max-Planck-Institut für extraterrestrische Physik, D-87545 Garching, Germany
[2] University of New Hampshire, Durham, NH 03824, USA
[3] University of California at San Diego, La Jolla, CA 92093, USA
[4] University of Iowa, Iowa City, IA 52242, USA
[5] University of Washington, Seattle, WA 98195, USA

Received: 8 March 1999 / Revised: 28 May 1999 / Accepted: 1 June 1999

Abstract. We present the first electron time-of-flight measurements obtained with the Electron Drift Instrument (EDI) on Equator-S. These measurements are made possible by amplitude-modulation and coding of the emitted electron beams and correlation with the signal from the returning electrons. The purpose of the time-of-flight measurements is twofold. First, they provide the drift velocity, and thus the electric field, when the distance the electrons drift in a gyro period becomes sufficiently large. Second, they provide the gyro time of the electrons emitted by the instrument, and thus the magnitude of the ambient magnetic field, allowing in-flight calibration of the flux-gate magnetometer with high precision. Results of both applications are discussed.

Key words. Magnetospheric physics (electric fields; plasma convection; instruments and techniques)

1 Introduction

The Electron Drift Instrument (EDI) was developed for ESA's Cluster mission. In view of its complexity, it was felt that a test-flight prior to Cluster would be highly desirable, and Equator-S was conceived largely for this purpose. Although Equator-S was delayed, the catastrophic loss of the Cluster mission on 4 June 1996 caused the original sequence to be restored. The goal of a full functional test of EDI was achieved in almost all respects, in spite of only 5 months of Equator-S operations. The present paper discusses EDI time-of-flight measurements of the electrons, while the companion paper (Quinn *et al.*, 1999) exploits the information contained in the beam firing-directions. After a brief description of the basis of the technique in Sect. 2, the operations and specific conditions on Equator-S are discussed in Sect. 3, before results of the time-of-flight measurements are presented in Sect. 4.

Correspondence to: G. Paschmann

2 Technique

The basis of the electron-drift technique is the injection of weak beams of 1-keV electrons and their detection after one or more gyrations in the ambient magnetic field. A detailed description of the technique may be found in two earlier publications (Paschmann *et al.*, 1997, 1998). Briefly, in the presence of a drift velocity v_d induced by an electric field $\mathbf{E}_\perp$ or a magnetic-field gradient ∇B, the circular electron orbits are distorted into cycloids. Their shape depends on whether the beam is injected with a component parallel or anti-parallel to the drift velocity. To be able to realise both types of orbits, EDI uses two guns and two detectors, as illustrated in Fig. 1. For each gun, only one orbit-solution exists that connects it with the detector on the opposite side of the spacecraft. Knowledge of the positions and firing directions of the guns, when their beams hit the detectors, uniquely determines the drift velocity. This is the basis of the triangulation technique employed in the companion paper by Quinn *et al.* (1999). Through triangulation, one directly determines the 'drift-step' which is the displacement of the electrons after a gyro time T_g:

$$d = v_d T_g \tag{1}$$

Note that for time-stationary conditions, one gun-detector pair would suffice, because the satellite spin would rotate the gun into all positions sequentially. This is essentially what was done with the Electron Beam Experiment on Geos-2, which served as the proof-of-principle for the electron-drift technique (Melzner *et al.*, 1978).

As is evident from Fig. 1, the two orbits differ in their length, and thus in the electron travel times. The electrons emitted with their velocity directed downstream, i.e., with a component parallel to v_d, have a time of flight that is shorter than T_g, while the electrons

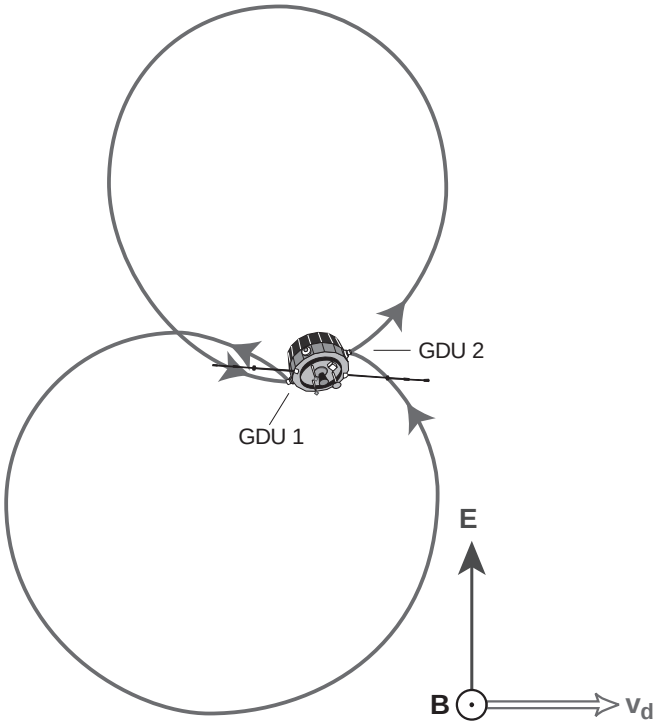

Fig. 1. EDI principle of operation. For any combination of magnetic field B and drift velocity v_d (assumed to be induced by an electric field E), only a single electron-trajectory exists that connects each gun with the detector on the opposite side of the spacecraft. The two trajectories have different path lengths and thus different times-of-flight. The drift velocity can be derived either from the two beam directions (triangulation technique), or from the difference in the travel times of the electrons (time-of-flight technique). Note that for clarity the electron orbits are drawn for an unrealistic combination of v_d and B

emitted upstream have a time of flight that is longer than T_g:

$$T_{1,2} = T_g(1 \pm v_d/v_e) \tag{2}$$

where v_e is the electron velocity.

From Eq. (2) it follows immediately that the sum of the two times is twice the gyro time:

$$T_1 + T_2 = 2T_g \tag{3}$$

while their difference is a measure of the drift velocity:

$$\Delta T = T_1 - T_2 = \pm 2(v_d/v_e)T_g = \pm 2d/v_e \tag{4}$$

We define T_1 and T_2 as the times-of-flight recorded by detectors 1 and 2, respectively. We have also chosen to number the gun and detector located in the same gun-detector unit (GDU) by the same number. Thus Gun 1, located in GDU 1 is aiming at Detector 2, located in GDU 2, and vice-versa. This makes ΔT a signed quantity. The plus sign indicates that the beam from Gun 2 to Detector 1 was directed upstream, while the beam from Gun1 to Detector 2 was directed downstream (and conversely for a negative ΔT). Noting that $T_g \propto 1/B$, it is evident that time-of-flight measurements allow B to be determined as well as v_d. The idea to use the difference in electron times-of-flight for electric field measurements is due to Tsuruda *et al.* (1985) and was first applied on Geotail (Tsuruda *et al.*, 1998).

EDI is the first instrument to combine the triangulation and time-of-flight techniques. Neither technique on its own could cover the full range of conditions on Equator-S or on Cluster. The triangulation technique is ideal for small values of the drift step d, i.e., when d is comparable to the triangulation base-line, which at most is twice the spacecraft diameter. This situation typically applies in regions of large magnetic fields. For large d, which typically occur in regions of small magnetic fields, the triangulation technique degenerates because d becomes large compared to the base-line. The time-of-flight technique shows the opposite behaviour. According to Eq. (4), ΔT increases with increasing d, and thus becomes easier to measure for large values of d. The two techniques therefore complement each other ideally. There is a region in parameter space where the two techniques overlap and can be compared.

In the magnetosphere, drift velocities never exceed a few thousand km s^{-1}, and more typically are a few km s^{-1} to a few hundred km s^{-1}, while the velocity of 1-keV electrons is 18742 km s^{-1}. According to Eq. (4), this implies that ΔT is only a small fraction of T_g, i.e., the drift introduces only a small variation in the two orbits and the associated times-of-flight. To make the difference visible, Fig. 1 is drawn for a very high drift velocity, v_d = 1000 km s^{-1}. The figure also uses an unrealistically large magnetic field, $B = 12$ μT, to be able to show the satellite and the electron orbits on the same scale. At such a large magnetic field, a drift velocity of 1000 km s^{-1} implies an electric field of 12 V m^{-1}. For realistic magnetic fields, the gyro radius is much larger, e.g., 1065 m for a 100 nT field.

In order to measure the electron times-of-flight, as well as to distinguish beam electrons from the background of ambient electrons that enter the detectors, the electron beams are amplitude-modulated with a pseudo-noise (PN) code. PN-codes are commonly used for measurements of signal propagation times. Nakamura *et al.* (1989) were the first to use a PN-code for drift measurements, in their case of ions. EDI employs a 15-chip code with a duration much shorter than T_g to achieve adequate time resolution. The electron time-of-flight is therefore equal to an integer number of code-lengths plus a fraction, of which only the fraction is measured by the correlators directly. However, by choosing an (initial) code-length equal to $T_g/5$, the number of complete wrap-arounds of the code can be recovered unambiguously, even if the errors in the magnetometer measurements (from which T_g is computed) were unexpectedly large and the electric-field-induced deviations from T_g had their maximum values. Once beam tracking has been achieved and the number of wrap-arounds established, the accuracy can be increased by gradually shortening the code-length, i.e., stepping down T_{chip}. To account for the large variations in T_g, the chip length T_{chip} can be varied between 238 ns and 122 μs.

Details of the EDI time-of-flight system and the beam-recognition and tracking schemes are more fully described in earlier publications (Vaith *et al.*, 1998; Paschmann *et al.*, 1998). Briefly, a set of 15 correlators

analyses the phasing of the detector counts relative to the beam code. Before beam acquisition has been achieved, all correlators will show the same counts (to within Poisson statistics) from the ambient electron background. Once the beam is acquired ('angle-track'), the correlator whose delay matches the electron flight-time will have the maximum number of counts. If the contrast between the correlated and uncorrelated counts exceeds some limit, the on-board software concludes that the beam has been acquired (see Sect. 4.3). A delay-lock-loop continuously shifts the code-phases of the correlators to keep the maximum centred in a specific channel ('time-track'). The code-shift step T_{step} was typically $T_{\text{chip}}/16$. By keeping track of the net change in code-phase, one obtains a measure of the changes in time-of-flight.

While the code-shift step T_{step} determines the precision of the time-of-flight measurements, their accuracy is ultimately limited by the chip length T_{chip}. Based on computer simulations of the EDI operation, the absolute accuracy has been estimated at about $1/5T_{\text{chip}}$. With a code-length set equal to $T_g/5$, the absolute accuracy of the individual time-of-flight measurements is thus $T_g/375$, or about 0.3% of T_g. Because T_g is equal to half the sum of the two times-of-flight, the relative accuracy $\delta T_g/T_g$ is then $\approx 0.2\%$. The same value applies to $\Delta T/(2T_g)$, the quantity which according to Eq. (4) determines v_d/v_e. For 1-keV electrons the error in v_d is thus about 35 km s^{-1}, independent of the magnitude of v_d. These error estimates hold for magnetic fields up to ≈ 2000 nT, because at this field strength the chip-length has reached its minimum value (238 ns) for a code that is $T_g/5$ long. Averaging will improve the accuracy at the expense of time resolution.

3 Operational characteristics and limitations

To find the beam directions that will hit the detector, EDI steps each beam in the plane perpendicular to **B** at a fixed angular rate (typically 0.1°/ms) until a signal has been acquired by the detector on the opposite side of the spacecraft. The direction of **B** is computed every 4 ms, based on the flux-gate magnetometer data available on board every 16 ms (Fornacon *et al.*, 1999). An accuracy of better than $\approx 1^\circ$ is required because the width of the beam is of this order. To account for arbitrary magnetic-field orientations, the guns are capable of firing in any direction within more than a hemisphere and the detectors can detect beams over an even larger range of directions. Once a signal has been acquired, the beams are swept back and forth to stay on target. The direction of the target changes constantly as a result of spacecraft spin and time variations in magnetic and electric fields. Because the flux-density of the returning beam strongly depends on B and on the highly variable background from ambient plasma electrons, beam currents are adjusted automatically over almost three orders of magnitude to maintain adequate signal and signal-to-noise ratio (SNR) levels. In spite of the adjustable beam currents, the signal or SNR can become too small for detection. However, this was generally not a problem on Equator-S.

The characteristics inherent in the EDI technique naturally pose limitations to its successful operation. There also are limitations that are specific to Equator-S. First, the beam-recognition algorithm that we had developed before launch and implemented in the on-board software was not optimal. In particular, it was triggered frequently by large fluctuations in background electron fluxes. This often kept the beams pointing in the wrong part of the $\mathbf{B}_\perp$-plane, causing large gaps between true beam hits, as illustrated by Fig. 3 in Quinn *et al.* (1999). Using high-rate data, we identified such false hits in ground software and developed and tested an improved on-board algorithm that will avoid this problem in future missions, such as Cluster-II. However, in low-rate data the detector count-rates that allow us to remove the false hits were not transmitted. For this reason our focus on Equator-S has been on high-rate data.

Second, Equator-S operated a set of magnetorquers during each perigee pass to slowly erect the spacecraft spin axis from its initial orientation in the ecliptic plane to an orientation normal to the ecliptic. This resulted in spacecraft stray fields of up to 1 nT that were different in magnitude and direction each time and could therefore not be corrected for in the on-board magnetometer data. Errors of order 1 nT are no concern to EDI if the total field is more than 100 nT, as in the companion paper (Quinn *et al.*, 1999). However, for fields of 50 nT or less, beam-pointing errors can become larger than the beam width, causing loss of track if the error moves the beam off of the $\mathbf{B}_\perp$-plane. This problem effectively limited successful operation on Equator-S to fields >30 nT, and all but eliminated the cases where the drift velocity became large enough to be measured by the time-of-flight technique. Ironically, the spin-axis erection manoeuvre was almost finished when the satellite was lost. Without torquer operation, the satellite stray field would have become sufficiently constant such that the resulting offsets could have been determined on the ground and included with the magnetometer calibration data that EDI employed on-board.

Third, the on-board software that would step down T_{chip} to increase the time-of-flight accuracy was never executed by the time the mission was over. Smaller values of T_{chip} tend to increase the susceptibility of the target tracking to temporal variations in magnetic and electric fields, and before these aspects had been adequately assessed, improvements of time-of-flight accuracy were considered less urgent.

4 Results

4.1 Gyro time measurements

From the average of the two times-of-flight, EDI can determine T_g, and thus B, with about 0.2% relative accuracy any time both beams are detected simultaneously and the magnetic field strength is less than

≈2000 nT. If the drift speed v_d is less than 100 km s^{-1}, the drift-induced deviation of either time-of-flight from T_g is less than 0.5%. In regions where v_d is not expected to exceed 100 km s^{-1}, one can therefore determine B with 0.5% relative accuracy even if only one of the beams is detected. The main application of the gyro-time measurements is in-flight calibration of the flux-gate magnetometer. Even small offsets along the satellite spin-axis can be determined precisely with these measurements.

Fig. 2 shows a comparison between the gyro times computed from the flux-gate measurements by the MAM instrument (Fornacon *et al.*, 1999) and the times-of-flight measured by EDI for a case where the magnetic field was 85 nT. The observed 12 μs discrepancy disappears if one assumes that there was in fact a 3.1 nT offset in the component along the satellite spin-axis. Once this offset was applied, the agreement became very good (better than 1%). The spin-offset remained fairly constant, as illustrated in the bottom part of Fig. 2 for data taken on a later date, but using the same offset. Similar comparisons have been performed for other times, with field magnitudes ranging from 29–122 nT. The lower the value of B, the better the absolute accuracy: at 30 nT, for example, the accuracy is ≈0.2 nT if T_g is measured to within 0.5%.

This method of determining spin-axis offsets requires that the cone-angle of the magnetic field relative to the spin-axis be sufficiently small, because under such circumstances much of the offset is directed parallel to **B** and thus adds to the total field strength. For cone-angles near 90°, however, the spin-axis offset is directed essentially transverse to **B** and the total field strength thus becomes insensitive to the offset.

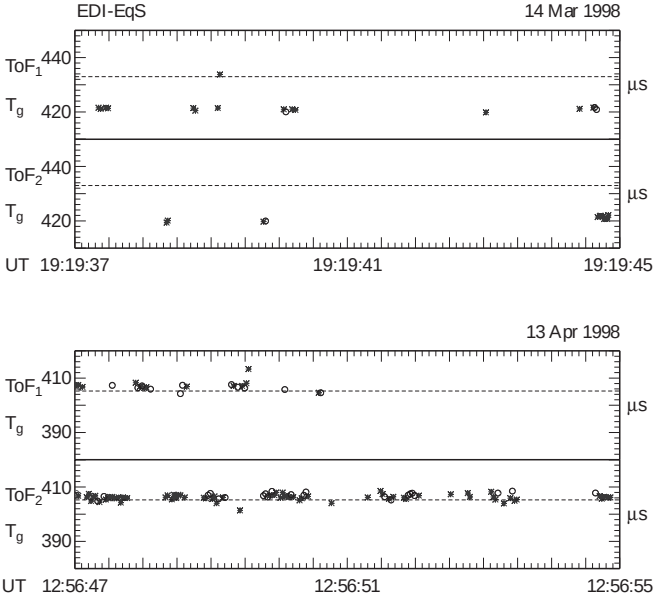

Fig. 2. Comparison of gyro-time measurements by EDI and the flux-gate magnetometer MAM for 8-s periods on 14 March 1998 (*top*) and for 13 April 1998 (*bottom*). The discrepancy of ≈12 μs between the time-of-flight measurements from EDI (*asterisks and circles*) and the gyrotime T_g computed from the field strength measured by MAM (*dashed line*) on 14 March can be attributed to a 3.1 nT spin-axis offset in the MAM data. The data for 13 April 1998 demonstrate good agreement (to within about 2 μs or 0.5%) after the 3.1 nT offset had been incorporated in the on-board computation

4.2 Multi-runners

Until now we have assumed that the beam electrons are detected after a single gyration. However, when sweeping the beams in the $\mathbf{B}_\perp$ plane, they might point in a direction that allows electrons to hit the detectors after two or more gyrations. For electrons having gyrated N times, the drift step becomes N times larger, and so does ΔT. This effect could be used to increase the accuracy of the drift measurements, if it were not for the fact that the return flux of the multi-runners drops sharply with increasing N, which restricts their probability of observation (as we later show). But knowledge of the number of gyrations is certainly important for the quantitative analysis of the data.

To tell how many times the detected electrons have actually gyrated, one only needs to check their times-of-flight. Fig. 3 shows a 0.25-s sequence with a rapid progression from single- to double- to eventually even quintuple-runners observed on 28 April 1998 at a time when the magnetic field was 285 nT. The time resolution was very high at this time because EDI was dumping data into its internal burst-memory at a rate of one sample every 4 ms, and reading it out at the normal telemetry rate later.

The identification of the multiplicity of the gyrations in Fig. 3 needs some explanation. As described earlier, the PN-code is much shorter than the gyro time. In this

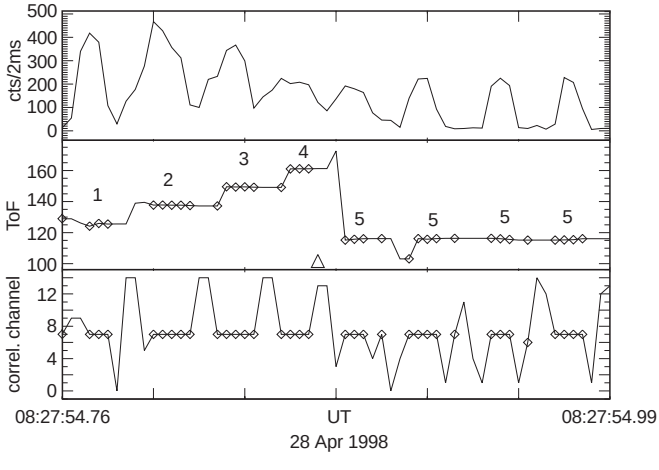

Fig. 3. Observations of electrons that have gyrated between one and five times, as indicated by the numbers in the *middle panel*. The figure shows, from *top to bottom*, the correlator counts accumulated in 2 ms; the apparent time-of-flight derived from the net code-shift (in μs); and the number of the correlator channel that the counts were recorded in. Channel number and time-of-flight are marked by *diamonds* if the counts appear in channel 7 ± 1, which is the tracking channel. The *triangular symbol* in the ToF panel marks the time of a correlator restart. As explained in the text, the ≈11.5 μs increment per added gyration is the gyro time modulo the code-length

particular case, the magnetic field was so strong that the chip-length was set to 1.9 μs, resulting in a code length of only 28.5 μs. The electrons having gyrated twice have therefore an apparent increment in time-of-flight of T_g modulo 28.5 μs relative to the single-runners. The same increment applies to each higher multiple. Inspection of Fig. 3 shows that the observed time-of-flight advances by ≈11.5 μs on average. The 11.5 μs, together with the code-length of 28.5 μs, implies that T_g was actually 125.5 μs, because 125.5 modulo 28.5 is 11.5. It is quite obvious that this method of distinguishing the multi-runners will work only as long as T_g is not itself a multiple of the code-length. Note also that we have assumed that drift velocities were so small that their effect on the times-of-flight could be ignored, a safe assumption in a magnetic field as strong as in the present case.

The progression from the quadruple- to the quintuple-runners in Fig. 3 is complicated by the fact that there was a correlator restart in-between (note triangular symbol). This restart was caused by the on-board software reacting to a poor tracking success by the other gun-detector pair. At such a restart, the code delay of the correlators is initialised so that single-runners would appear in channel 7. However, immediately after the restart the gun was actually pointing at the quintuple-runner target, and the time-of-flight thus was $4T_g$ larger. At 11.5 μs per step, four steps would advance the time-of-flight by 46 μs. Taken modulo 28.5 μs, this gives a drop in apparent time-of-flight of 11 μs, as observed.

Another aspect of the multi-runners concerns the observed flux levels. The electron beams have a finite angular width, and thus spread along **B** linearly with increasing path-length, and thus with increasing number of gyrations. In the $\mathbf{B}_\perp$-plane, on the other hand, the beams are refocussed after each T_g. If the drift-step is small compared with the gun-detector spacing, as is the case for this example, the fluxes recorded by the detectors should therefore decrease almost linearly with the number of gyrations. However, Fig. 3 shows some deviations from the expected behaviour. While the count-rates for the double-, triple-, and quadruple-runners show the expected linear progression, the single-runners have less flux than the double-runners, and the quintuple-runners have higher fluxes than the quadruple-runners. The likely explanation for these discrepancies is the beam-profile. When performing the angular scan of the beam, the centre of the beam-profile will not be precisely in the $\mathbf{B}_\perp$-plane, but may wander off by some fraction of a degree. This angle-offset will in general be different for the electrons with different number of gyrations. As the beam intensity falls off rapidly with angular distance from the beam-centre, this intensity variation can mask variations resulting from longer path-lengths.

Note that Fig. 3, while serving to illustrate the method of identifying multi-runners, is an extreme case. When magnetic fields drop below 100 nT or so, usually only single-runners are observed. This is because for drift-steps that are large compared with the gun-detector separation, the return fluxes should scale as the square of the number of gyrations, making multi-runners hard to detect.

4.3 Drift velocity measurements

From the discussion in Sect. 2, drift velocities must exceed ≈35 km s^{-1} to become detectable from individual measurements of the times-of-flight T_1 and T_2, given the conservative choice of the code-chip length employed on Equator-S. However, such high drift velocities usually occur only in low magnetic fields, and such generally pose a problem for EDI on Equator-S, because of the magnetorquer-induced offsets in the magnetometer readings. The apogee pass on 12 April 1998 was an exception because drift speeds of 30 to almost 50 km s^{-1} occurred in 35 to 50 nT fields. The corresponding drift step was in the range 30–45 m and thus still measurable by the triangulation technique. This situation provided the first opportunity to compare the two complementary methods.

Fig. 4 shows a 4-s period on 12 April that illustrates the character of the high-rate telemetry data. The panels labelled Max_1 and Max_2 show the counts (per 2 ms) recorded by the correlator channels (labelled MaxCh_1 and MaxCh_2) having the maximum number of counts in Detectors 1 and 2, respectively. Data are sampled

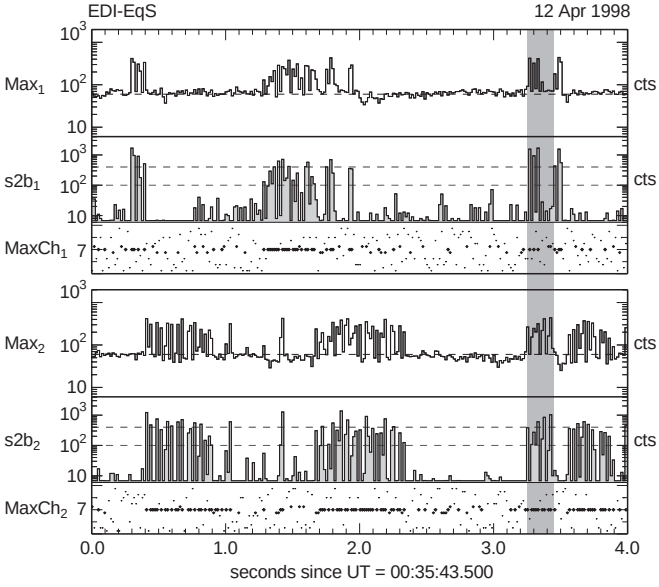

Fig. 4. Detector data for a 4-s period near apogee on 12 April when the magnetic field was 48 nT. The *top three panels* are for Detector 1: Max_1 shows the maximum counts (per 2 ms) recorded by any of the 15 correlators in Detector 1, and MaxCh_1 the correlator channel that received the maximum counts. The quantity $\mathrm{s2b}_1$ is the square of the signal-to-noise ratio (SNR) computed from the counts in the correlators. If $\mathrm{s2b}_1$ exceeds the threshold indicated by the *lower dashed line*, the on-board software assumes that the beam from Gun 2 has been detected by Detector 1; MaxCh_1 then indicates the correlator whose delay matches the time-of-flight of the beam electrons; when $\mathrm{MaxCh}_1 = 7$, time-track has been achieved. (If $\mathrm{s2b}_1$ exceeds the *upper dashed line*, this is used internally as a measure of the highest signal quality). The next three panels repeat the same information for Detector 2. The *shaded area* highlights the time interval discussed in Figure 5

internally every 2 ms and transmitted to the ground every 16 ms. During periods of beam hits, $MaxCh_1$ and $MaxCh_2$ indicate the channels whose time-delay matches the time-of-flight of the electrons, modulo the code-length. When the signal appears in Channel 7, time-track has been achieved. The baseline levels of about 60 are the counts from the ambient background electrons. The times when the beams return to their detectors are clearly recognisable as count levels of several hundred. However, the on-board software does not identify beam hits from the changes in the count-rates directly, but from a quantity s2b, which is an estimate of the square of the beam counts, divided by the background counts from ambient electrons, i.e., the instantaneous SNR^2. This quantity is computed continuously from the counts recorded simultaneously in the matched and unmatched correlator channels every 2 ms. If s2b exceeds the threshold indicated by the lower dashed line for two samples in a row, this is taken as evidence that the beam is returning to the detector. The threshold was 100 in this case, implying a SNR of 10, but values up to almost 2000 (SNR $\approx$ 45) are observed, indicating that signal levels were more than adequate. The fact that the beam hits appear as bursts, with gaps up to 1 s or so in between, is due to the noted problems with the tracking algorithms and the magnetometer readings on Equator-S.

Fig. 5 shows an example where we have superimposed the results from the time-of-flight measurements onto those from triangulation. The format of the plot is the same as in the accompanying paper by Quinn *et al.* (1999). The figure shows gun locations and firing directions for a 0.2-s interval during which the beams were aimed at a point about 30 m distant. During this 0.2-s interval there were three valid measurements of T_1 and eight measurements of T_2. The difference, ΔT, between the averaged times-of-flight was 3.35 μs, with a mean error of 0.9 μs. The gyro time T_g was 750 μs. Converting these numbers into a drift step, $d = \Delta T v_e/2$, one obtains (31.5 ± 8) m, in good agreement with the triangulation results.

It is important to note that according to Eq. (4), ΔT is a signed quantity. For the case in Fig. 5, Gun 2 was actually firing at the target, while Gun 1 was firing away from it. According to Eq. (4), this should produce a positive ΔT, as observed. Thus the agreement is not simply in magnitude but also in sign.

Fig. 6 shows another comparison between time-of-flight and triangulation results. The figure is for a 0.4-s interval during which the satellite spin moved Gun 1 enough to provide an adequate baseline all by itself. This was necessary because Gun 2 was not tracking well at this time (only one hit during this interval). The dispersion of the triangulation results, indicated by the circular symbols, is to be expected for triangulation of such a large drift-step from an (effective) baseline that is only 3 m long. During the 0.4-s interval, there were ten measurements of T_2, but only a single measurement of T_1. The difference ΔT between the single T_1 and the averaged T_2 was −4.64 μs, and the gyro time T_g was 1044 μs. The chip-length was 15.3 μs at this time, implying an error in ΔT of about 2 μs. The observed times imply a drift step of (43.5 ± 20) m. The agreement with the

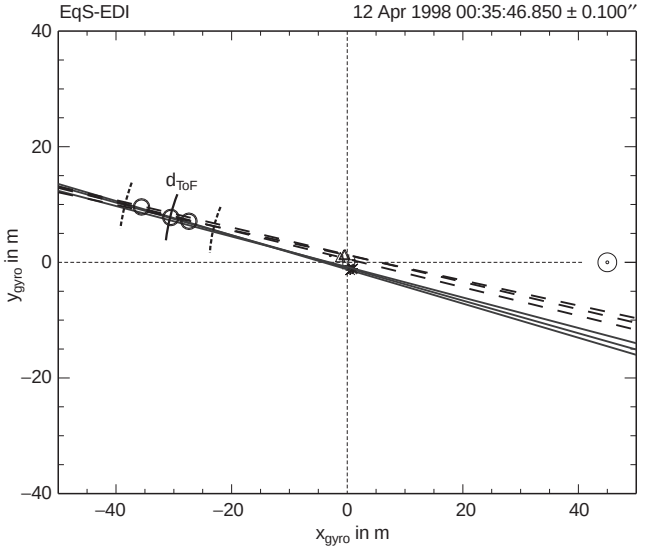

Fig. 5. Comparison of triangulation and time-of-flight results. The figure shows the gun locations, projected into the gyro-plane (x_{gyro}, y_{gyro}), and the firing directions, for the 0.2-s interval marked by the *grey-shading* in Fig. 4. *Solid straight lines* indicate the firing directions from Gun 1 (*crosses*), *dashed lines* those from Gun 2 (*triangles*). Triangulation of the drift step, based on these directions and a correction for curvature of the electron trajectories, yields the positions marked by the *open circles*. The drift step calculated from the measured difference in the times-of-flight (31.5 m) is indicated by the *line* marked d_{ToF}, and the error of the mean by the neighbouring *dashed lines*. A drift step of 31.5 m corresponds to a drift velocity of 42 km s^{-1}, equivalent to an electric field of 2.0 mV m^{-1}. The drift is directed to the right, or sunward, as indicated by the sun-symbol

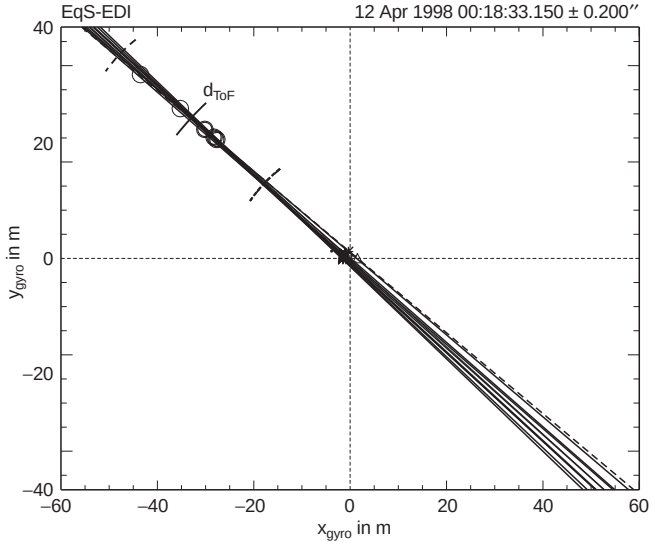

Fig. 6. A second comparison of triangulation and time-of-flight results for a 0.4-s interval near 00:18:33 UT on the same day. The format is the same as that of Fig. 5, except for a scale change. Triangulation (*circular symbols*) implies a drift step of 35–55 m, in fair agreement with the (43.5 ± 20)m calculated from the difference between the times-of-flight. The magnetic field was only 35 nT in this case, and so the measured drift step corresponds to a drift velocity of 42 km s^{-1}, equivalent to an electric field of 1.5 mV m^{-1}

triangulation results is quite good, given the large uncertainty in both measurements at this time. The negative sign of ΔT agrees with expectations because Gun1 was firing at the target, while Gun 2 was firing away from it.

Fig. 7 shows a final comparison, for a 0.2 s interval near 00:56:20 UT on the same day. Triangulation gave a drift step of only (20 ± 5) m, while the time-of-flight measurements gave (35 ± 10) m, derived from a difference of (-3.75 ± 1.0) μs, obtained from the averages over four and three measurements of T_1 and T_2, respectively. A drift step of order 25 m is clearly close to the limit of the time-of-flight measurements, even with averaging, and thus it is not surprising that the two methods barely overlap. However, note that the negative sign agrees with the beam pointing-directions implied by the triangulation result.

5 Summary

We have demonstrated in this paper that EDI is able to make precise time-of-flight measurements of its beam electrons. These measurements have several applications. First, the electron gyro time T_g, and thus B, can be measured with an accuracy better than 1% for magnetic fields larger than about 2000 nT. An application of this ability, which does not even require continuous tracking or particularly tight timing, is the precise determination of the spin-axis offset in the flux-gate magnetometer data, provided the magnetic field is not always oriented transverse to the satellite spin axis. This new method to determine spin-axis offsets solves a problem that commonly plagues the flux-gate measurements.

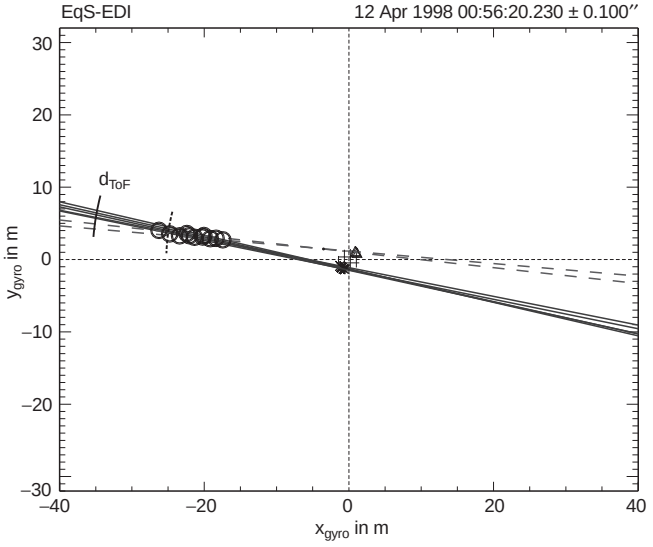

Fig. 7. A third comparison of triangulation and time-of-flight results, for a triangulation drift step of only (20 ± 5)m that just overlaps with the drift step derived from the difference in averaged times-of-flight, (35 ± 10)m, of which only the average, labeled d_{ToF} and the lower error bound are shown. The magnetic field was 40 nT at this time

The observation of electrons that have gyrated several times before they hit the detectors serves to demonstrate the internal consistency of the EDI measurements. In principle, the increased drift-steps and increased differences in times-of-flight of multi-runners provide an opportunity to improve the accuracy of the measurements. Because of the longer flight paths and consequent reduced flux of the multi-runners, however, they typically are observed only in the strongest magnetic fields.

The most important application of the time-of-flight measurements is the determination of the electron drift velocity, and thus the electric field, from the difference ΔT between the times-of-flight of the two beams. Because this difference is proportional to the drift step d, it is easier to measure for larger values of d. Thus the time-of-flight technique complements the triangulation technique, which deteriorates when d becomes large compared to the triangulation baseline. We have demonstrated with a few examples that, for drift steps in the range 30–50 m, both techniques give similar results. The accuracy of the ΔT measurements was limited to 30–50% in the examples shown. To get a better cross-calibration of the two techniques in this range of drift steps, the sensitivity and accuracy of the time-of-flight measurements needs to be higher than had been achieved by the time Equator-S was lost. This requires reducing the code-chip length without sacrificing beam tracking, so that smaller ΔTs can be determined reliably. Only the Cluster mission will show whether this goal can be achieved.

For larger drift steps, of order 100 m or larger, the settings used on Equator-S would have been adequate. Such large drift steps imply drift velocities of 100 km s^{-1} or more. Drift velocities of this magnitude either did not occur during the times of successful EDI operations, or they occurred in low magnetic fields, where EDI operations on Equator-S were compromised by the problems with beam pointing caused by the residual magnetic fields of the magnetorquers.

Acknowledgements. The authors would like to thank the many people who have made the EDI experiment possible through years of development, testing, and operational support, in particular B. Briggs, R. Frenzel, S. Frey, W. Göbel, J. Googins, G. King, R. Maheu, F. Melzner, U. Pagel, P. Parigger, D. Simpson, K. Strickler, and C. Young. We owe great thanks to the spacecraft team at MPE, especially H. Höfner, F. Melzner, P. Parigger, and J. Stöcker, as well as to the mission operations team at DLR/GSOC, in particular T. Kuch and A. Braun. This work was supported by DLR through grant 50OC89043 and by NASA through grant NAG5-6935. The Equator-S project was supported by DLR through grant 50OC94024.

The Editor-in-Chief thanks K. Tsuruda and A. Balogh for their help in evaluating this paper.

References

Fornacon, K.-H., H. U. Auster, E. Georgescu, W. Baumjohann, K.-H. Glaßmeier, J. Rustenbach, and M. Dunlop, The magnetic field experiment onboard Equator-S and its scientific possibilities, *Ann. Geophys.*, **17,** 1999.

Melzner, F., G. Metzner, and D. Antrack, The Geos electron beam experiment, *Space Sci. Rev.*, **4,** 45, 1978.

Nakamura, M., H. Hayakawa, and K. Tsuruda, Electric field measurement in the ionosphere using the time-of-flight technique, *J. Geophys. Res.*, **94,** 5283–5291, 1989.

Paschmann, G., F. Melzner, R. Frenzel, H. Vaith, P. Parigger, U. Pagel, O. H. Bauer, G. Haerendel, W. Baumjohann, N. Sckopke, R. B. Torbert, B. Briggs, J. Chan, K. Lynch, K. Morey, J. M. Quinn, D. Simpson, C. Young, C. E. McIlwain, W. Fillius, S. S. Kerr, R. Maheu, and E. C. Whipple, The Electron Drift Instrument for Cluster, *Space Sci. Rev.*, **79,** 233–269, 1997.

Paschmann, G., C. E. McIlwain, J. M. Quinn, R. B. Torbert, and E. C. Whipple, The electron drift technique for measuring electric and magnetic fields, in R. F. Pfaff, J. E. Borovsky, and D.T. Young (eds.), *Measurement Techniques in Space Plasmas: Fields*, pp. 29–38, Geophysical Monograph 103, American Geophysical Union, Washington, DC, 1998.

Quinn, J. M., G. Paschmann, N. Sckopke, V. K. Jordanova, H. Vaith, O. H. Bauer, W. Baumjohann, W. Fillius, G. Haerendel, S. S. Kerr, C. A. Kletzing, K. Lynch, C. E. McIlwain, R. B. Torbert, and E. C. Whipple, EDI convection measurements at 5–6R_E in the post-midnight region, *Ann. Geophys*, **17,** 1999.

Tsuruda, K., H. Hayakawa, and M. Nakamura, in A. Nishida (ed.) Science Objectives of the Geotail Mission, p. 234, ISAS, Tokyo, 1985.

Tsuruda, K., H. Hayakawa, and M. Nakamura, Electric field measurements in the magnetosphere by the electron beam boomerang technique, in R.F. Pfaff, J.E. Borovsky, and D.T. Young (eds.), *Measurement Techniques in Space Plasmas: Fields*, pp. 39–45, Geophysical Monograph 103, American Geophysical Union, Washington, DC, 1998.

Vaith, H., R. Frenzel, G. Paschmann, and F. Melzner, Electron gyro time measurement technique for determining electric and magnetic fields, in R.F. Pfaff, J.E. Borovsky, and D.T. Young (eds.), *Measurement Techniques in Space Plasmas: Fields*, pp. 47–52, Geophysical Monograph 103, American Geophysical Union, Washington, DC, 1998.